Creating Three Pentacoordinated Carbons in a Six-Membered Ring. An Atoms-in-Molecules and Electron-Localization Function Study on the Trishomocyclopropenyl Cation and Phosphorus, Sulfur, Arsenic, and Selenium Analogues

Nick Henry Werstiuk* and Yi-Gui Wang

Department of Chemistry, McMaster University, Hamilton, Ontario L8S 4M1, Canada

Received: June 11, 2003; In Final Form: August 22, 2003

The trishomocyclopropenyl cation and related species were investigated at the Becke3PW91/6-311G(d,p) and MP4(SDQ)/6-311G(d,p) levels of theory. The bonding was characterized on the basis of atoms-in-molecules (AIM) theory, as well as in terms of basins and their populations within the electron-localization function (ELF) framework. There are no pentacoordinated carbons in the trishomocyclopropenyl cation, although it is stabilized by σ,σ-no-bond homoconjugation; it is not a hypercoordinate species. Only when the C1−C3, C3−C5, and C1−C5 distances are fixed at 1.576 Å is a σ,σ-bond homoconjugated species obtained, but it is not a stationary point and is 21.7 kcal mol^{-1} higher in energy than the equilibrium-optimized trishomocyclopropenyl cation. When the methylene groups of the trishomocyclopropenyl cation are replaced with PH, S, AsH, and Se, equilibrium-optimized σ,σ-bond homoconjugated species that exhibit three pentacoordinated carbons are obtained. A rationale for these observations is presented.

Introduction

The concept of homoaromaticity was first introduced by Winstein in 1959 to explain the acetolysis behavior of *cis*-3-bicyclo[3.1.0]hexyl toluenesulfonate (**1**).[1] The formation of an

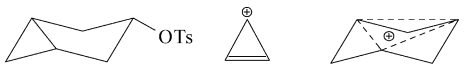

1 **2** **3**

intermediate of C_{3v} symmetry was used to account for the anchimeric acceleration, the deuterium scrambling at C1, C3, and C5, the cis stereochemistry of the products, the lack of olefin formation, and the special salt effect observed in its acetolysis.[2] It was named the trishomocyclopropenyl cation (we use the acronym **THCPC** herein), the prefix indicating the number of CH_2 groups intervening between the carbon atoms of the cyclopropenyl cation **2**, which is aromatic. **THCPC** was also prepared as a long-lived species under superacid conditions.[3,4] The concept of homoaromaticity had the undeniable effect of directing much experimental and theoretical attention to the field.[5−8] The usual representation of **THCPC** with dotted lines shown as **3** suggests that it bears three pentacoordinated carbons. Like the so-called "nonclassical" 2-norbornyl cation—in fact, we have established that 2-norbornyl also is not a pentacoordinate species at C6—**THCPC** was also employed by Olah to advance hypercarbon chemistry[9] with the proposal that a trisynaptic dotted line be used to represent "3c−2e" bonds. Although these dotted-line representations are widely accepted by many chemists to this point, we should be aware that these additional "bonds" are drawn only for convenience and it is important to have a correct picture of the nature of bonding defined on a rigorous basis. Two orbital-independent methods, the quantum theory of atoms-in-molecules (AIM)[10,11] and the electron-localization function (ELF) method[12] meet this requirement.

AIM uses the electron density $\rho(\mathbf{r})$ as the information source, and chemical concepts are formulated through analysis of its gradient vector field. Two atoms are covalently bonded if their nuclei are linked via a bond path (BP), a line of maximum electron density with respect to neighboring lines between nuclei.[10] The bond critical point is the "communication point" between two atoms, and bonds can be characterized from properties evaluated at the bond critical point (BCP). The coordination number of an atom is defined as the number of bond paths terminating at the nucleus, and the *molecular structure* of a molecule is a connectivity scheme—the molecular graph—governed by the topology of $\rho(\mathbf{r})$. In AIM theory, the partitioning of Cartesian space into regions (atomic basins) demarcated by zero-flux surfaces in the electron density results in open quantum-mechanical subsystems the properties of which satisfy all fundamental relations such as the (hyper)virial and Ehrenfest theorems. Also, the integration of the Fermi hole density at HF level within a single basin and between two basins will separately yield the localization index ($\lambda(A) = |F(\Omega,\Omega)|$) and the delocalization index ($\delta(A,B) = 2|F(\Omega,\Omega')|$).[13,14]

The ELF method involves a topological analysis of the gradient vector field of the Becke−Edgecombe electron localization function (ELF)[12] as implemented by Silvi and coworkers.[15] In ELF, core basins are organized around nuclei (with $Z > 2$) providing an inner-atomic-shell-like structure, and valence basins occupy the remaining space. In the ELF picture, bonding is defined on the basis of how valence basins interact with core basins, that is, the number of core basins that a valence basin is stuck on.[16] A small basin population and a large basin fluctuation ($\lambda > 0.5$) indicates a high delocalization, and a contribution analysis can show how the basins are delocalized. Integration of the one-electron density $\rho(\mathbf{r})$ and of the pair function $\pi(\mathbf{r}_1,\mathbf{r}_2)$ over the volume Ω of one basin provides the basin population $\bar{N}$ and its variance σ^2, which is the contribution from other basins to $\bar{N}$. The relative fluctuation $\lambda = \sigma^2/\bar{N}$ provides an indication of the delocalization within that basin, while a contribution analysis gives a quantitative measure of

* To whom correspondence should be addressed.

10.1021/jp030741x CCC: $25.00
Published on Web 10/07/2003

TABLE 1: Geometrical Parameters and Relative Energies at the Becke3PW91/6-311G(d,p) Level

cation[a]	C,C[c] (Å)	C,X[b,c] (Å)	X,X[b,c] (Å)	angle sum (deg)	deviation (deg)	ΔE (kcal mol^{-1})
THCPC	1.832	1.486	2.581	360	25.1	
	(1.836)	(1.493)	(2.594)	(360)	(24.9)	
e-THCPC−PH	1.820	1.851	3.217	357.8	7.7	0.0
	(1.830)	(1.850)	(3.231)	(358.3)	(7.9)	(0.0)
a-THCPC−PH	1.863	1.830	3.318	358.9	9.0	−9.4[d]
	(1.868)	(1.832)	(3.317)	(358.8)	(8.7)	(−10.2)
THCPC−S	1.821	1.774	3.104	358.5	10.4	
	(1.818)	(1.774)	(3.106)	(358.6)	(10.3)	
e-THCPC−AsH	1.778	1.984	3.459	355.7	7.9	0.0
a-THCPC−AsH	1.813	1.965	3.560	357.0	8.1	−6.0[e]
THCPC−Se	1.809	1.923	3.378	357.1	8.7	

[a] C_{3v} symmetry not enforced for these optimizations. [b] X is the heavy atom (C)H$_2$, (P)H, S, (As)H, and Se. [c] The data in parentheses were obtained at the MP4(SDQ)/6-311G(d,p) level. [d] With the inclusion of ZPE, the value is −8.6 kcal mol^{-1}. [e] With the inclusion of ZPE, the value is −5.6 kcal mol^{-1}.

TABLE 2: Total and Relative Energies (kcal mol^{-1}) as a Function of C,C Distance (Å) at Becke3PW91/6-311G(d,p) Level

C,C[a]	**THCPC**	**e-THCPC−PH**	**a-THCPC−PH**	**THCPC−S**	**e-THCP−AsH**	**a-THCPC−AsH**	**THCPC−Se**
1.5	−233.63442(41.9)	−1141.46383(29.8)	−1141.47067(34.9)	−1310.14116(33.7)	−6825.05960(21.6)	−6825.06261(25.7)	−7320.24487(27.4)
1.6	−233.67401(17.1)	−1141.49295(11.5)	−1141.50236(15.0)	−1310.17390(13.2)	−6825.08277(7.0)	−6825.08829(9.6)	−7320.27226(10.2)
1.7	−233.69381(4.6)	−1141.50676(2.9)	−1141.51849(4.9)	−1310.18968(3.3)	−6825.09227(1.1)	−6825.10000(2.2)	−7320.28480(2.3)
1.8	−233.70080(0.3)	−1141.51116(0.1)	−1141.52509(0.7)	−1310.19477 (0.1)	−6825.09385(0.1)	−6825.10350(0.04)	−7320.28834(0.1)
1.9	−233.69962(1.0)	−1141.50981(0.9)	−1141.52605(0.11)	−1310.19323(1.1)	−6825.09082(2.0)	−6825.10226(0.8)	−7320.28662(1.2)
2.0	−233.69266(5.4)	−1141.50475(4.1)	−1141.52345(1.7)	−1310.18737(4.7)	−6825.08505(5.6)	−6825.09824(3.3)	−7320.28170(4.3)
2.1	−233.68145(12.4)	−1141.49743(8.7)	−1141.51874(4.7)	−1310.17894(10.0)	−6825.07787(10.1)	−6825.09284(6.7)	−7320.27520(8.3)
2.2	−233.66615(22.0)	−1141.48826(14.5)	−1141.51241(8.7)	−1310.16857(16.5)	−6825.06975(15.2)	−6825.08658(10.7)	−7320.26786(13.0)
opt[b]	−233.70121(0.0)	−1141.51131(0.0)	−1141.52623(0.0)	−1310.19491(0.0)	−6825.09398(0.0)	−6825.10356(0.0)	−7320.28851(0.0)
LDBP[c]	−233.66660(21.7)	−1141.50905(1.4)	−1141.52605(0.11)	−1310.19468(0.14)	−6825.08090(8.2)	−6825.09618(4.6)	−7320.28288(3.5)

[a] The homoconjugating carbon atoms. C_{3v} symmetry was enforced in these calculations. [b] The optimized C,C distance is 1.832, 1.820, 1.863, 1.821, 1.778, 1.813, and 1.809 Å for **THCPC**, **e-THCPC−PH**, **a-THCPC−PH**, **THCPC−S**, **e-THCPC−AsH**, **a-THCPC−AsH**, and **THCPC−Se**, respectively. C_{3v} symmetry not enforced for these optimizations (See Table 1). [c] The largest C,C distance exhibiting a bond path: 1.576, 1.920, 1.900, 1.849, 2.06, 2.04, and 1.980 Å for **THCPC**, **e-THCPC−PH**, **a-THCPC−PH**, **THCPC−S**, **e-THCPC−AsH**, **a-THCPC−AsH**, and **THCPC−Se**, respectively.

SCHEME 1

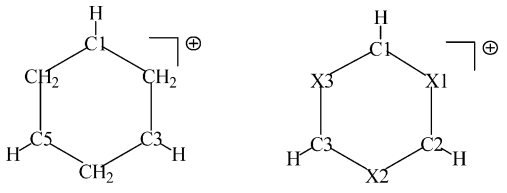

THCPC

THCPC-PH, X = PH
THCPC-S, X = S
THCPC-AsH, X = AsH
THCPC-Se, X = Se

the contributions of other specific basins to the variance σ^2 on a percentage basis.[16,17]

Cremer, Bader, and co-workers were the first researchers to describe homoaromaticity on the basis of AIM theory.[18] Later Cremer and co-workers carried out a systematic investigation of a number of homoaromatic species[19] and concluded that **THCPC** was among the species that are stabilized—according to the Cremer classification—by σ,σ-no-bond homoconjugation.[20] But no examples that possess σ,σ-bond homoconjugation were reported.[8,20] Our burgeoning interest in studying so-called nonclassical cations with AIM and ELF[21−24] led us to reexamine **THCPC** and study a number of its analogues. In this paper, we report our results on AIM and ELF investigations of **THCPC** and its analogues **THCPC−PH**, **THCPC−S**, **THCPC−AsH**, and **THCPC−Se** in which the methylenes of **THCPC** are replaced with PH, S, AsH, and Se groups as shown in Scheme 1.

Computations

Becke3PW91 and MP4(SDQ) calculations were carried out with Gaussian 94[25] on SGI Octane and SGI Origin 2000 computers and with Gaussian 98[26] on a Cray T90. In earlier studies on homoaromaticity, the geometries were often optimized at the MP2/6-31G(d) level of theory, and single-point energies were occasionally calculated at the MP4(SDQ)/6-31G(d) level.[20] We have established that calculations with the Becke3PW91 hybrid functional yield geometries close to those obtained at the MP2(full) level with the same basis sets at a much lower computational cost.[21−24] Consequently, the Becke3PW91/6-311G(d,p) level of theory was employed to obtain optimized geometries—selected parameters are collected in Table 1—and wave functions throughout this study. The total energies are given in Table 2. To test the validity of using this level, optimizations at the MP4(SDQ)/6-31G(d) level were also carried out in selected cases. The studies of electronic charge density $\rho(\mathbf{r})$, its gradient vector field $\nabla\rho(\mathbf{r})$, and its Laplacian ($\nabla^2\rho(\mathbf{r})$), as well as integrations, were carried out with the AIMPAC suite of programs[27] with the appropriate wave function. AIM2000 was used to obtain the molecular graphs.[28] The sign of $\nabla^2\rho(\mathbf{r})$ at a BCP is usually a good indicator of the bond character; negative values indicate covalent bonds, and positive values indicate ionic bonds.[10,11] The Laplacian can also reveal the atomic shell structure.[10] Nevertheless, it is also found that $\nabla^2\rho(\mathbf{r})$ alone is insufficient as a probe for assigning covalent bond character especially when the bonds exhibit near-zero or very small electron densities at the BCPs; $\nabla^2\rho(\mathbf{r})$ may also miss the outer shell structure of heavy atoms. On the other hand, the local electronic energy density ($E_d(\mathbf{r}) = G(\mathbf{r}) + V(\mathbf{r})$, where $G(\mathbf{r})$ and $V(\mathbf{r})$ are the kinetic energy and the potential energy densities),[29] as well as the one-electron potential (OEP),[30] can be employed in these cases. We also include $E_d(\mathbf{r})$ and OEP results in this paper**.** Displays of the one-electron potential (OEP) were obtained with GRIDV2 (we modified GRIDV[10] of

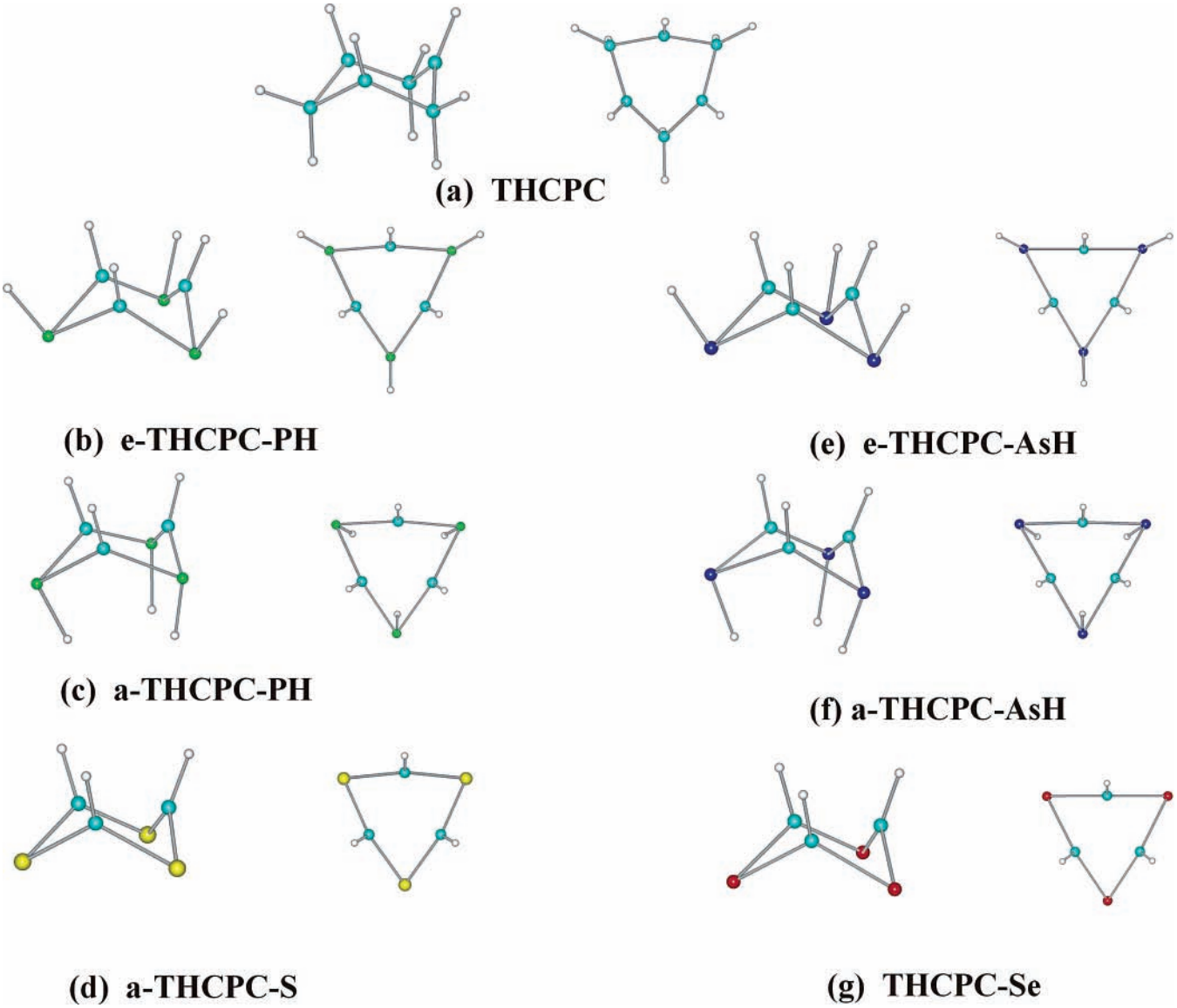

Figure 1. Displays of two orientations of equilibrium-optimized geometries of (a) **THCPC**, (b) **e-THCPC−PH**, (c) **a-THCPC−PH**, (d) **THCPC−S**, (e) **e-THCPC−AsH**, (f) **a-THCPC−AsH**, and (g) **THCPC−Se** at the Becke3PW91/6-311G(d,p) level.

AIMPAC), which can additionally deal with the OEP and the virial, and CONTOUR. We used the AIMDELOC program[31] to calculate the localization and delocalization indices (LIs and DIs) from the Becke3PW91/6-311G(d,p) atom overlap matrix (AOM) obtained from AIMPAC integrations. While the HF level was recommended for calculating LIs and DIs because the Fermi hole is the sole source of correlation between electrons at HF level,[14] we also include analyses at the HF/6-311G(d,p)// Becke3PW91/6-311G(d,p) level. ELF calculations with wave functions obtained at Becke3PW91/6-311G(d,p) level were carried out with Silvi's TopMod package.[32,33] To check for basis set dependence,[23] wave functions obtained at Becke3PW91/cc-pVTZ//Becke3PW91/ 6-311G(d,p) level were also analyzed. A box size that extended 3.0 au from the outermost atomic coordinates in each direction and a step size of 0.1 au were typically used. Additional details on the ELF calculations can be found in ref 23. The results were visualized with SciAn.[34]

Results and Discussion

In all of the discussions, we use X as the symbol for CH_2, PH, S, AsH, and Se and C refers to the carbons that are involved in homoconjugation. In **THCPC**, the carbons are numbered from C1 to C6. The numbering of atoms (in **THCPC**, the corresponding atoms are C1, C3, and C5), C,C distance(s), and fold angle are defined in Scheme 2. These numberings are applicable for all tables including the basin contributions in Tables 4 and 5. The only exception is the numbering for Tables 12 and 13, in which **THCPC** takes the naming of substituted molecules for convenience.

SCHEME 2

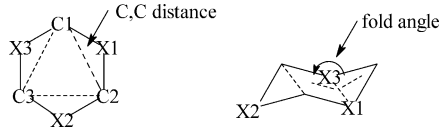

Geometries. Optimized equilibrium structures of C_{3v} cations **THCPC**—the distance between the homoconjugated carbons (HOMCCs) is 1.832 Å—and its analogues **THCPC−PH**, **THCPC−S**, **THCPC−AsH**, and **THCPC−Se** obtained at the Becke3PW91/6-311G(d,p) are displayed in Figure 1. The phosphorus and arsenic species, **THCPC−PH** and **THCPC−AsH**, exhibit two conformations in which the hydrogens are equatorial (Figure 1b,e) and axial (Figure 1c,f). The prefixes e- and a- refer to the isomers in which the hydrogens are equatorial

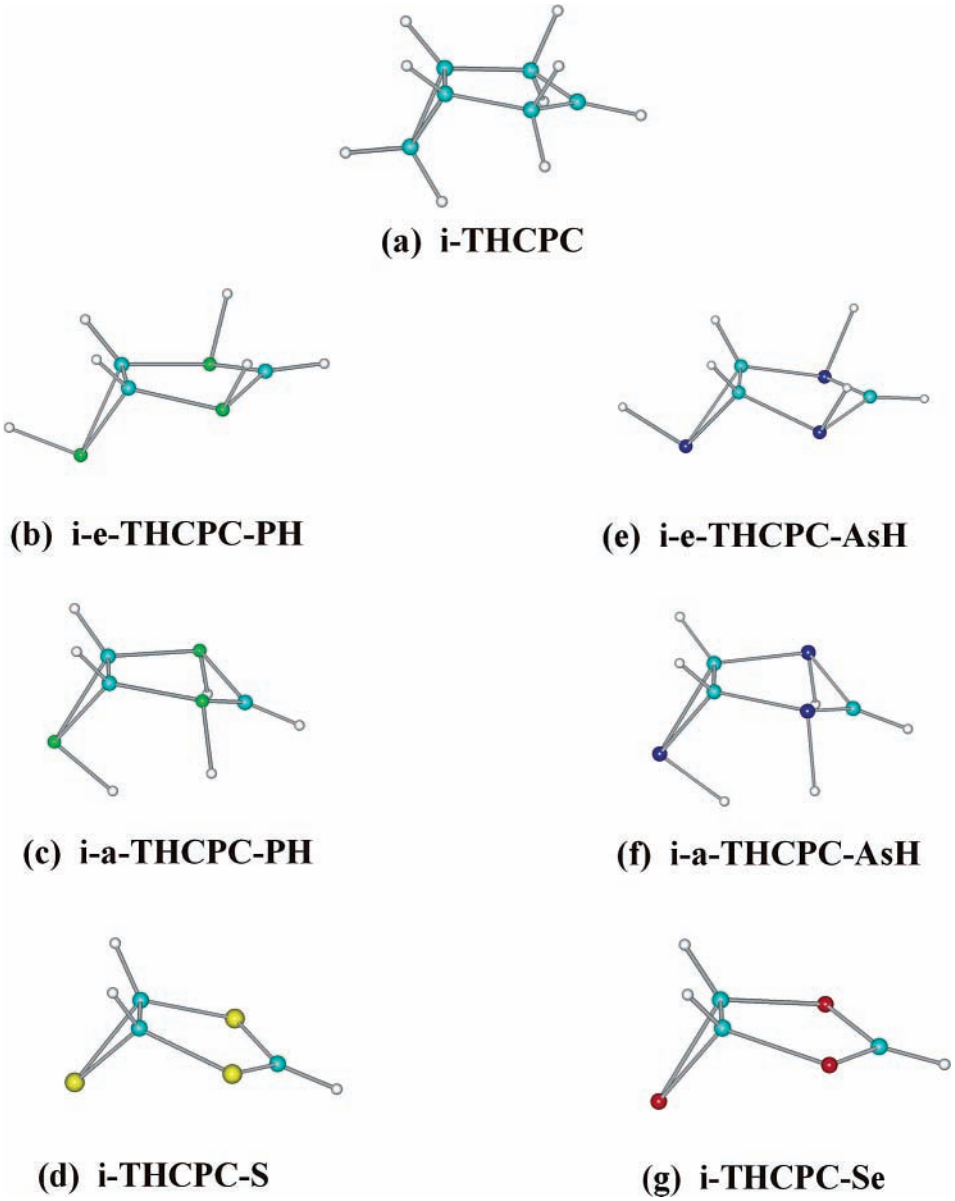

Figure 2. Displays of equilibrium-optimized geometries of (a) **i-THCPC**, (b) **i-e-THCPC−PH**, (c) **i-a-THCPC−PH**, (d) **i-THCPC−S**, (e) **i-e-THCPC−AsH**, (f) **i-a-THCPC−AsH**, and (g) **i-THCPC−Se** at the Becke3PW91/6-311G(d,p) level.

and axial, respectively. Selected geometrical parameters obtained at the Becke3PW91/6-311G(d,p) and MP4(SDQ)/6-311G(d,p) levels are collected in Table 1. That the parameters are virtually identical at these two levels of theory supports our view that the Becke3PW91/6-311G(d,p) level is suitable for studying homoaromatic species. Entries in column five of this table give the sum of three bond angles around HOMCC C1 (C3 and C5). For C1, this sum is ∠H−C1−X1 + ∠H−C1−C3 + ∠X1−C1−X3. A value close to 360° indicates that three bonds around these carbons nearly lie in a plane. According to the p-orbital model,[6] a p orbital is perpendicular to this plane and the angle formed by the p orbital and the C1−C3−C5 plane is listed as the deviation in the adjacent column in Table 1. We expect that homoconjugation should be facilitated as the deviation angle approaches 0°. In this case, the p-orbitals that are directed toward each other lie in the same plane and overlap is maximized. **THCPC** has the largest deviation angle of 25.1°, and the other species have values that range between 7.7° and 10.4°. The distances between the HOMCCs in all species range between 1.778 and 1.868 Å, and the C−X (X = CH_2) distances are much shorter than the C1,C3(C5) distance(s) in **THCPC**. In e-**THCPC−PH**, a-**THCPC−PH**, and **THCPC−S**, the C1,C2(C3) and C−X distances are similar in magnitude in the range of 1.8 Å. In e-**THCPC−PH**, the C−X distances are slightly longer than C1,C2(C3) distances by 0.030 Å. As far as e-**THCPC−AsH**, a-**THCPC−AsH**, and **THCPC−Se** are concerned, the C−X distances are significantly longer (0.114−0.206 Å) than C1,C2(C3) distances. In the case of **THCPC−PH** and **THCPC−AsH**, the axial isomers are lower in energy than the equatorial isomers by 8.6 and 5.6 kcal mol^{-1}, respectively.

We also found that the C_{3v} cations isomerize to the 3-bicyclo-[3.1.0] species **i-THCPC**, **i-e-THCPC−PH**, **i-a-THCPC−PH**, **i-THCPC−S**, **i-e-THCPC−AsH**, **i-a-THCPC−AsH**, and **i-THCPC−Se** displayed in Figure 2. As was the case for the homoconjugated species, two conformations were found for the phosphorus (Figure 2b,c) and arsenic species (Figure 2e,f).

AIM Molecular Structure. As reported by Cremer,[18] we find no bond paths between C1, C3, and C5 of **THCPC** at all levels of theory, so there are no pentacoordinated carbons in this carbocation. The molecular graph of **THCPC** is displayed as Figure 3a. The plots of $\rho(\mathbf{r})$ and $\nabla^2\rho(\mathbf{r})$ in the HOMCC plane are given in Figure 4, panels a and b, respectively. The electron

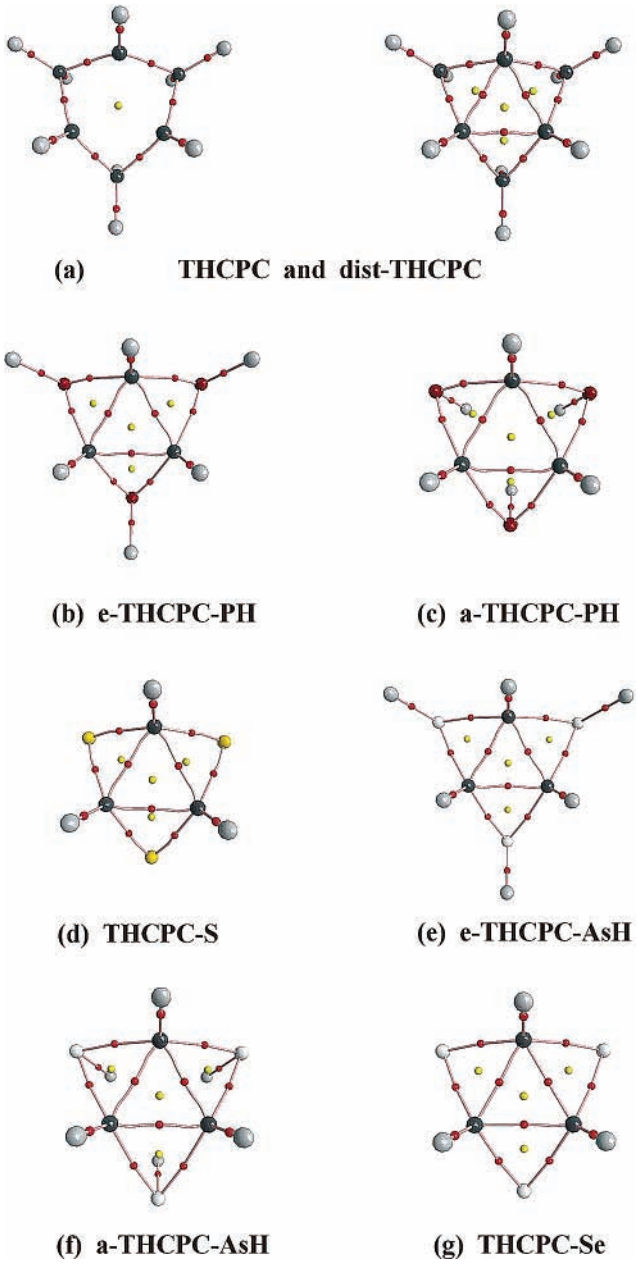

Figure 3. Displays of molecular graphs of (a) **THCPC** and **dist-THCPC**, (b) **e-THCPC−PH**, (c) **a-THCPC−PH**, (d) **THCPC−S**, (e) **e-THCPC−AsH**, (f) **a-THCPC−AsH**, and (g) **THCPC−Se**.

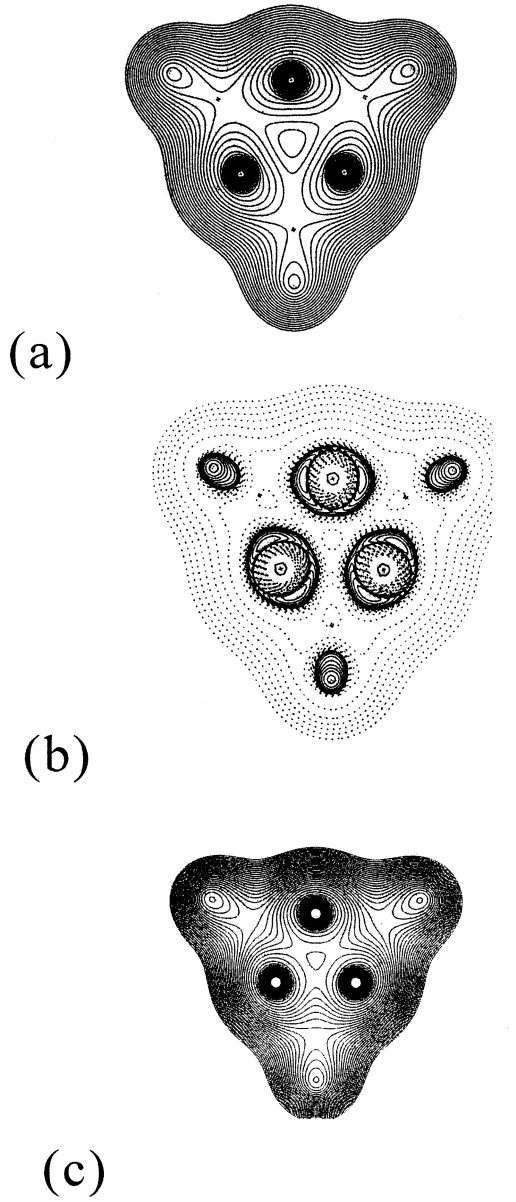

Figure 4. Display of (a) $\rho(\mathbf{r})$ (outer contour, 0.01) in the C1−C3−C5 plane of **THCPC** at the Becke3PW91/6-311G(d,p) level, (b) $\nabla^2\rho(\mathbf{r})$, and (c) $\rho(\mathbf{r})$ (outer contour, 0.01) in the C1−C3−C5 plane of **dist-THCPC**.

density is obviously concentrated around carbon centers, and there are essentially holes rather than lumps in $\nabla^2\rho(\mathbf{r})$ pointing to other carbons. Virtually identical plots (not displayed) were obtained at a higher level of theory (Becke3PW91/cc-pVTZ//Becke3PW91/6-311G(d,p)). Only when the C1−C3, C3−C5, and C1−C5 distances are fixed at 1.576 Å is a σ,σ-bond homoconjugated—this is the Cremer terminology[19]—species with BPs between the HOMCCs realized. The molecular graph and a plot of $\rho(\mathbf{r})$ in the HOMCC plane are displayed as **dist-THCPC** in Figure 3a and Figure 4c, respectively. The saddle points in $\rho(\mathbf{r})$ between the HOMCCs are clearly seen in Figure 4c. But, this species, which is *21.7 kcal mol*$^{-1}$ *higher in energy* than the equilibrium-optimized **THCPC**, is not a stationary point. That **dist-THCPC** is topologically unstable is not surprising given the proximity of the BCPs to the ring critical points (RCPs).

When the CH_2 groups of **THCPC** are replaced with PH or S, yielding **e-THCPC−PH**, **a-THCPC−PH**, and **THCPC−S**, bond paths are found between the HOMCCs at the Becke3PW91/6-311G(d,p) level, as seen in the molecular graphs displayed as Figure 3b−3d. Three pentacoordinated carbons are present in the six-membered rings at this level. Figure 5a,c,e (Supporting Information) displays $\nabla^2\rho(\mathbf{r})$ in the HOMCC plane overlaid with the bond paths for **e-THCPC−PH**, **a-THCPC−PH**, and **THCPC−S**. The properties at BCPs and RCPs, along with the distances between the RCPs and BCPs, are given in Table 3. The RCP2s are the additional RCPs that are formed when bond paths (BPs) are formed between C1−C2(C3). Noteworthy is the fact that the differences in electron density at the BCPs and RCPs in the HOMCC plane are small (0.013 and 0.014 e Å^{-3}) and the distances between BCPs and RCPs are also small (0.291 and 0.212 Å) in **a-THCPC−PH** and **THCPC−S** (Figure 3c,d); the ellipticities at the BCPs are large (3.072 and 3.548). These data indicate that **a-THCPC−PH** and **THCPC−S** are topologically unstable. A small increase in the internuclear distances or decrease in electron density between the HOMCCs should result in an annihilation of the critical

TABLE 3: Properties at Bond and Ring Critical Points at the Becke3PW91/6-311G(d,p) Level

cation	BCP/RCP	$\rho(\mathbf{r})$ (e Å^{-3})	$\nabla^2\rho(\mathbf{r})$ (e Å^{-5})	$E_d(\mathbf{r})$ (e Å^{-5})[a]	ϵ[b]	distance (Å)[c]
THCPC	C−X	1.707	−13.544	−5.350	0.164	
	RCP1	0.661	1.735	−0.771		
e-THCPC−PH	C−C[d]	0.844	0.410	−1.374	1.707	0.488
	C−X	0.952	−1.663	−3.133	0.236	
	RCP1	0.709	1.470	−0.843		
	RCP2	0.776	2.193	−1.133		
a-THCPC−PH	C−C[d]	0.776	1.301	−1.133	3.072	0.291
	C−X	0.985	−1.229	−3.253	0.276	
	RCP1	0.628	1.904	−0.651		
	RCP2	0.763	2.506	−0.988		
THCPC−S	C−C[d]	0.844	1.060	−1.350	3.548	0.212
	C−X	1.242	−6.434	−3.374	0.006	
	RCP1	0.709	1.446	−0.868		
	RCP2	0.830	3.061	−1.133		
e-THCPC−AsH	C−C[d]	0.903	−0.692	−1.618	1.011	0.703
	C−X	0.804	0.792	−1.564	0.230	
	RCP1	0.781	1.330	−1.020		
	RCP2	0.654	3.541	−0.797		
a-THCPC−AsH	C−C[d]	0.840	−0.135	−1.404	1.058	0.644
	C−X	0.831	0.688	−1.665	0.214	
	RCP1	0.713	1.592	−0.839		
	RCP2	0.659	3.331	−0.792		
THCPC−Se	C−C[d]	0.850	−0.058	−1.444	1.334	0.563
	C−X	0.947	−0.125	−1.910	0.025	
	RCP1	0.734	1.380	−0.888		
	RCP2	0.724	3.516	−0.874		

[a] The local electronic energy density ($E_d(\mathbf{r})$) is defined as $E_d(\mathbf{r}) = G(\mathbf{r}) + V(\mathbf{r})$, where the $G(\mathbf{r})$ and $V(\mathbf{r})$ correspond to the local kinetic and potential energy densities, respectively. [b] The ellipticity ϵ is defined as $\lambda_1/\lambda_2 - 1$. [c] The distance between BCP and RCP2, which is the newly formed ring critical point. [d] The homocongugated carbons.

points. This expectation is borne out at the Becke3PW91/cc-pVTZ//Becke3PW91/6-311G(d,p) level; **a-THCPC−PH** (Figure 5d) and **THCPC−S** (Figure 5f) lose the C1−C2(C3) bond paths. Only in **e-THCPC−PH** (Figure 5b) are they retained at this level. Bond paths are also found in **e-THCPC−AsH**, **a-THCPC−AsH**, and **THCPC−Se** as seen in Figure 3, parts e,f, and g, respectively, identifying them as hypercoordinate species. However, these cations differ from the PH and S analogues in that $\nabla^2\rho(\mathbf{r})$ is negative at the bond critical points (Table 3), although the value is close to zero in **a-THCPC−AsH** and **THCPC−Se**. Cations **e-THCPC−AsH**, **a-THCPC−AsH**, and **THCPC−Se** exhibit larger differences in density between RCPs and BCPs (0.118−0.249 e Å^{-3}) and longer distances between the RCPs and BCPs (0.488−0.703 Å). This is clearly seen in Figure 3e−g. Moreover, the ellipticities (1.011−1.707) are smaller further indicating that **e-THCPC−AsH**, **a-THCPC−AsH**, and **THCPC−Se** (this is also the case in **e-THCPC−PH**) are more stable topologically than **a-THCPC−PH** and **THCPC−S**. That the C1−C2(C3) bond paths persist at the Becke3PW91/cc-PVTZ//Becke3PW91/6-311G(d,p) level in these cations is consistent with the expected topological stability based on the positions of the BCPs and RCPs. The local electron energy densities[10] ($E_d(\mathbf{r}) = (G(\mathbf{r}) + V(\mathbf{r}))$ at all BCPs and RCPs are negative. According to Cremer[29] ($E_d(\mathbf{r})$ was defined as $H(\mathbf{r})$), $H(\mathbf{r})$ is <0 for covalent bonds but not for "ionic" bonds or bonds arising from van der Waals interactions.

Unlike the case of **e-THCPC−PH**, **a-THCPC−PH**, and **THCPC−S** (see Figure 5a,c,e), we found that the nonbonded charge concentrations (NBCCs) are not recovered in $\nabla^2\rho(\mathbf{r})$ for **e-THCPC−AsH** (Figure 6a; the charge concentrations of the equatorial As−H bonds are seen in this case), **a-THCPC−AsH**, (Figure 6c), and **THCPC−Se** (Figure 6e). Figure 6 is included as Supporting Information. This is better seen in the side-view plots of $\nabla^2\rho(\mathbf{r})$ in the C1−As−C2 and C1−Se1−C2 planes displayed in Figure 7, parts a,c, and e, respectively. Figure 7 is also included as Supporting Information. On the other hand, contour plots of the OEP in the HOMCC plane, displayed as Figure 6b,d,f, clearly show the NBCCs associated with the lone

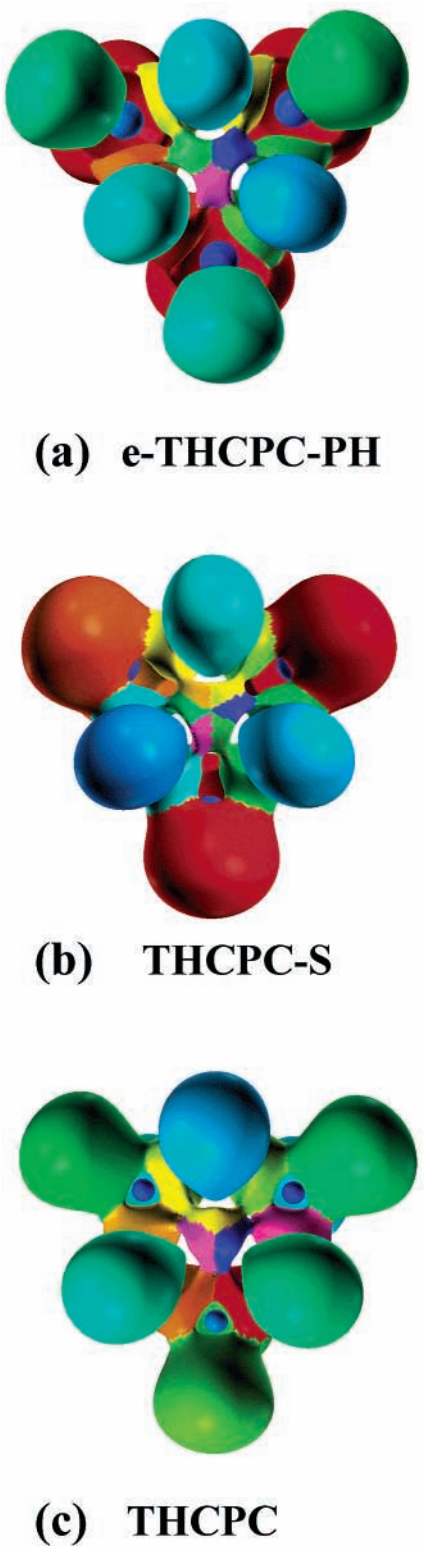

Figure 8. Display of ELF basins (0.60 contour) in the C1−C2−C3 plane of (a) **e-THCPC−PH** at the Becke3PW91/6-311G(d,p)//Becke3PW91/6-311G(d,p) level, (b) **THCPC−S** at the Becke3PW91/6-311G(d,p)//Becke3PW91/6-311G(d,p) level, and (c) **THCPC** at the Becke3PW91/cc-PVTZ//Becke3PW91/6-311G(d,p) level.

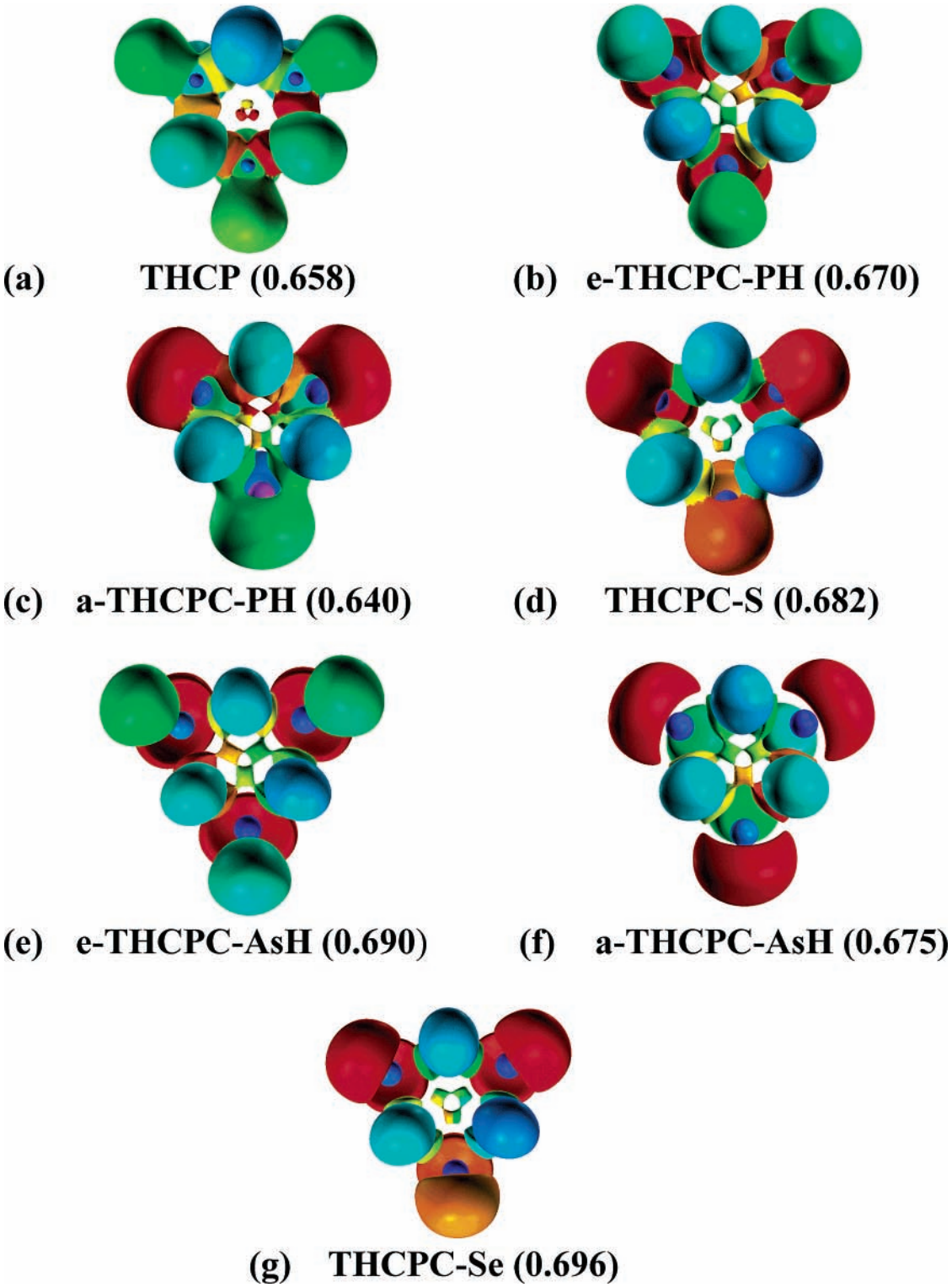

Figure 9. Display of ELF basins at the bifurcation contour value at Becke3PW91/6-311G(d,p)//Becke3PW91/6-311G(d,p) level unless specified otherwise: (a) **THCPC** at the Becke3PW91/cc-PVTZ//Becke3PW91/6-311G(d,p) level; (b) **e-THCPC−PH**; (c) **a-THCPC−PH**; (d) **THCPC−S**; (e) **e-THCPC−AsH**; (f) **a-THCPC−AsH**; (g) **THCPC−Se**.

pairs.[30] The corresponding side-view OEP plots of **e-THCPC−AsH**, **a-THCPC−AsH**, and **THCPC−Se** are displayed as Figure 7b,d,f.

ELF Structure. The ELF plots displayed in Figures 8 and 9 clearly show large basins on P, S, As, and Se that can be interpreted as lone pairs, but the number of basins and their connections in the HOMCC plane differ from species to species and are basis-set dependent. These results show the difficulties that can arise in ELF analyses. Three types of ELF structures are found for these cations as displayed in Figure 8 (the hydrogens attached to the HOMCCs are colored blue). The first case is seen in **e-THCPC−PH** at the Becke3PW91/6-311G-(d,p) level, for which there are disynaptic basins between the HOMCCs (Figure 8a). The **e-** and **a-THCPC−As** cations exhibit very similar ELF structures at Becke3PW91/6-311G-(d,p) except that the basins are trisynaptic and not disynaptic. The second case is seen in **THCPC−S**, which shows six monosynaptic basins in the HOMCC plane at the same level

TABLE 7: Delocalization Indices δ(A,B) at the Becke3PW91/6-311G(d,p) Level

cation	C,C[a]	C,X	C,H	$\sum\delta$(A,B)[b]	e-X,H	a-X,H
THCPC	0.477 (0.478)	0.987 (0.976)	0.917 (0.931)	3.845 (3.839)	0.920 (0.931)	0.921 (0.932)
e-THCPC−PH	0.677 (0.697)	0.781 (0.702)	0.926 (0.946)	3.842 (3.744)	0.854 (0.776)	
a-THCPC−PH	0.648 (0.672)	0.788 (0.702)	0.929 (0.951	3.801 (3.699)		0.832 (0.753)
THCPC−S	0.523 (0.540)	1.077 (1.061)	0.884 (0.901)	4.084 (4.107)		
e-THCPC−AsH	0.650 (0.658)	0.845 (0.810)	0.923 (0.940)	3.913 (3.876)	0.953 (0.927)	
a-THCPC−AsH	0.621 (0.632)	0.857 (0.817)	0.927 (0.947)	3.883 (3.845)		0.936 (0.908)
THCPC−Se	0.573 (0.585)	1.023 (1.006)	0.892 (0.909)	4.084 (4.091)		

[a] The values in parentheses obtained at the HF/6-311G(d,p)//Becke3PW91/6-311G(d,p) level. [b] Only five pairs, two C,C, two X,X, and C,H, included.

(Figure 8b); roughly one-half of the species that we studied exhibit this feature. **THCPC** is the third case; at the Becke3PW91/cc-pVTZ//Becke3PW91/6-311G(d,p) level, three monosynaptic basins are found in the HOMCC plane (Figure 8c). **THCPC−S** also exhibits this structure at the Becke3PW91/cc-pVTZ level. As seen in Figure 8, all small basins in the HOMCC plane share separatrixes. Figure 9 is a display of the ELF plots at the bifurcation values of the small basins. It is noteworthy that the ELF basins are not concentrated at the center of the HOMCC plane in any of the cations. Except for **THCPC** and **THCPC−S** at the Becke3PW91/cc-pVTZ//Becke3PW91/6-311G(d,p) level, all of the cations have basins remaining between carbons and the bifurcation values are very close to the attractor values as seen from the η values collected in Tables 4 and 5 (Supporting Information).

AIM Delocalization Indices and Properties of ELF Basins. AIM atomic charges are given in Table 6 (Supporting Information). The data were obtained at the Becke3PW91/6-311G(d,p)//Becke3PW91/6-311G(d,p) and HF/6-311G(d,p)//Becke3PW91/6-311G(d,p) levels with the latter values shown in parentheses in the tables. Although all of the species are cations, the carbon atoms bear a negative charge, while the P, As, S, and Se atoms are positively charged. The HF method increases the charge separation. Not unexpectedly, the hydrogens on the HOMCCs also bear significant positive charge. On the whole, the atomic charges are qualtitatively similar at the HF and Becke3PW91 levels. Delocalization indices—we use the acronyms LI and DI for the localization and delocalization indices, respectively, in the text of this paper for convenience—are collected in Table 7. The LIs (F(A,A), Table 8) differ significantly from species to species and range from 3.992 to 4.834. On the other hand, the sum of the DIs ($\sum\delta_{A,B}$) between one carbon and all other atoms remains virtually constant between 4.100 and 4.228. The $\delta_{C,X}$ contributions are dominant parts of $\sum\delta_{A,B}$ for **THCPC**, **THCPC−S**, and **THCPC−Se**, while their contributions are comparable to the $\delta_{C,Cs}$ in **e-THCPC−PH**, **a-THCPC−PH**, **e-THCPC−AsH**, and **a-THCPC−AsH**. Relative to the HF results, the DI values of $\delta_{C,C}$ and $\delta_{C,H}$ are smaller and those of $\delta_{C,X}$ are larger at the Becke3PW91 level showing that this DFT treatment appears to reduce the electron density between carbon atoms. As for the DIs of the bonding pairs and other C,C pairs in the cations, the values of $\delta_{C,C}$ in **e-** and **a-THCPC−PH** and **e-** and **a-THCPC−AsH** cations are larger than those in **THCPC−S** and **THCPC−Se** cations, which in turn are larger than those in **THCPC**. The values of $\delta_{C,X}$ exhibit the reverse trend. The Becke3PW91 method reduces $\delta_{C,C}$ ($\delta_{C,H}$) and increases $\delta_{C,X}$. Overall, the results obtained at the HF and DFT levels are similar. The degree to which the current DFT methods include the Coulomb-correlation effect is under evaluation. We have proposed a practical method to calculate DIs at post-HF levels of theory and assessed the Coulomb-correlation effect as determined with the currently used correlation methods.[35]

Properties of the small ELF basins in the HOMCC plane and the V(C,X) basins are collected in Tables 4, 5, and 9, respectively. Although the number of basins and the synaptic properties vary from species to species and exhibit a basis-set dependence, the properties of the basins are similar. The basins associated with the HOMCC planes have populations in the region of 0.37−0.64 e, of which 84−95% exchange with other basins on the basis of the values of λ. The values are not significantly different at the Becke3PW91/cc-pVTZ//Becke3PW91/6-311G(d,p) level (cf. Table 5). A contribution analysis shows that V(C,H) and the two V(C,X) basins (V(C,H)) around the carbon are the dominant contributors to the C1, C3, and C5 basins. The in-plane basins have small η values (0.655−0.735) and very small volumes (4.22−6.10 bohr^3). The direct contributions of the lone pairs on the X atoms to the populations of these small basins are negligible. The other small basins in the HOMCC plane also contribute only marginally to the small basins. The V(C,X) basins have populations close to 2 (1.57−1.93), and the attractors of the V(C−X) basins have η values close to 1 (0.889−0.944). About 54−63% of the populations come from other basins, the lone pairs or V(C,H) basins on X or both making the largest contributions.

Hypercoordination. Even though bond paths (atomic interaction lines) are found between C1−C3, C3−C5, and C1−C5 of **THCPC** when the C1,C3(C5) distances are reduced to 1.576 Å, this triple-hypercoordinate species, which is not a stationary point, is 21.7 kcal mol^{-1} higher in energy than equilibrium-optimized **THCPC** (Table 2). In Table 2, C_{3v} symmetry is enforced, and all of the parameters except C,C distance are optimized. In the case of **a-THCPC−PH** and **THCPC−S**, the bond paths disappear when the HOMCC distances are increased (the energies increase marginally by 0.11 and 0.14 kcal mol^{-1}) only slightly by 0.03 and 0.029 Å in keeping with the fact that the BCPs and RCPs are close to the annhilation point and the BCPs and BPs are lost when the large correlation-consistent basis set cc-pVTZ is used. In the case of **e-THCPC−PH**, the distances must be increased by 0.101 Å (the energy increases by 1.4 kcal mol^{-1}) to lose the bond paths. The variation of the energy as a function of the HOMCC distance for **e-THCPC−PH**, **a-THCPC−PH**, and **THCPC-S** is shown graphically in Figure 10. Figure 10 was obtained from independent calculations and exactly has the same potential energy curve as that obtained from data in Table 2. In the case of the **e-THCPC−AsH**, **a-THCPC−AsH**, and **THCPC−Se**, the distances must be increased by 0.281, 0.227, and 0.171 Å, the energy increases being 8.2, 4.6, and 3.5 kcal mol^{-1}, respectively.

It is clear that **a-THCPC−PH** and **THCPC−S** are boundary species topologically, pentacoordination being lost when the cc-pVTZ basis set is used to obtain the wave function. The instability of these boundary species is also seen in the large ellipticities (3.1 and 3.5) at BCPs and small distances between BCPs and RCPs (0.2−0.3 Å). That a slight opening of these C_{3v} cations, an increase of only 0.14 and 0.11 kcal mol^{-1}, results in a loss of the pentacoordination provides further evidence that hypercoordination is tenuous in these species. All of the cations that we investigated exhibit a high degree of delocalization in

TABLE 8: Cationic carbon properties at the Becke3PW91/6-311G(d,p) Level

cation	$\|F(A,A)\|^a$	localization (%)^b	$\sum\delta(A,B)^c$	pair contribution (%)
THCPC	3.992	66.1	4.100	23.2 C,C; 48.2 C,X; 22.4 C,H; 1.3 C···X
	(4.045)	(66.4)	(4.089)	(23.4 C,C; 47.8 C,X; 22.8 C,H; 1.1 C···X)
e-THCPC−PH	4.762	69.5	4.179	32.4 C,C; 37.4 C,X; 22.2 C,H; 5.0 C···H(X); 1.4 C···X
	(4.968)	(70.8)	(4.105)	(34.0 C,C; 34.2 C,X; 23.0 C,H; 6.0 C···H(X); 1.1 C···X)
a-THCPC−PH	4.834	69.9	4.154	31.2 C,C; 38.0 C,X; 22.4 C,H; 5.0 C···H(X); 2.1 C···X
	(5.044)	(71.3)	(4.063)	(33.0 C,C; 34.6 C,X; 23.4 C,H; 6.0 C···H(X); 1.6 C···X)
THCPC−S	4.107	66.0	4.228	24.8 C,C; 51.0 C,X; 20.9 C,H; 2.5 C···X
	(4.209)	(66.6)	(4.226)	(25.6 C,C; 50.2 C,X; 21.3 C,H; 2.0 C···X)
e-THCPC−AsH	4.457	68.1	4.168	31.2 C,C; 40.5 C,X; 22.1 C,H; 1.8 C···X
	(4.576)	(68.9)	(4.131)	(31.9 C,C; 39.2 C,X; 22.8 C,H; 1.5 C···X)
a-THCPC−AsH	4.489	68.4	4.150	29.9 C,C; 40.3 C,X; 22.3 C,H; 2.3 C···X
	(4.616)	(69.2)	(4.104)	(30.8 C,C; 39.9 C,X; 23.1 C,H; 1.8 C···X)
THCPC−Se	4.243	66.7	4.235	27.3 C,C; 48.3 C,X; 21.1 C,H; 2.6 C···X
	(4.331)	(67.2)	(4.219)	(27.7 C,C; 47.0 C,X; 21.5 C,H; 2.1 C···X)

[a] The values in parentheses were obtained at the HF/6-311G(d,p)//Becke3PW91/6-311G(d,p) level. [b] The percent localization, $(F(A,A)/\bar{N}) \times 100$. [c] The sum over all possible pairs between the carbon atom and other atoms.

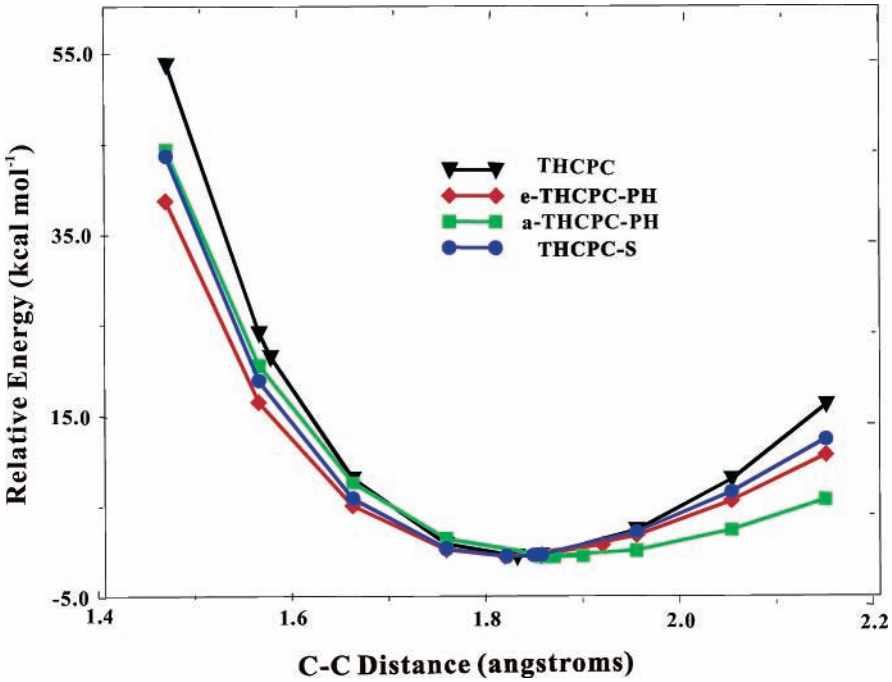

Figure 10. The relationship between the relative energy and the HOMOCC distances for **THCPC**, **THCPC−S**, **THCPC−PH**, and **THCPC−S** with C_{3v} symmetry at Becke3PW91/6-311G(d,p)//Becke3PW91/6-311G(d,p) level.

HOMCC plane. The DIs between the HOMCCs are always larger than 0.477. The values of ρ at the RCPs are not significantly smaller than the values at the BCPs between the HOMCCs.

In keeping with this is the fact that the small ELF basins in the HOMCC plane exhibit large fluctuations—λ is greater than 0.80 in every case—and many basins contribute to the fluctuations. While the ELF values of the attractors of these tiny basins are small (0.655−0.745), the ELF values at which they bifurcate from the other basins are substantial (Figure 9) but only slightly smaller than η (Tables 4 and 5) in keeping with the fact that the electrons are delocalized in the HOMCC plane. While Walsh orbitals are used to account for the surface delocalization[5,19,20] p-orbital overlaps are often employed to explain homoaromaticity.[6,36] However, Walsh orbitals cannot be obtained by a unitary transformation of the bonding manifold of doubly occupied cyclopropane canonical MOs.[37,38] In the case of **THCPC**, both orbital models imply that electrons would concentrate in the center of the HOMCC plane because orbital overlap is expected to the largest at that point. However, AIM shows that a RCP is located at the center of the surface. Even in **THCPC** (Becke3PW91/cc-PVTZ//Becke3PW91/6-311-G(d,p)) and **THCPC−S** (Becke3PW91/6-311-G(d,p)//Becke3PW91/6-311-G(d,p)) in which one monosynaptic basin is found for each carbon as seen in Figures 8a,b and 9a,b, the attractors of the basins are not at the center of the HOMCC plane. When there are six monosynaptic basins, the ELF value at which bifurcation of the two monosynaptic basins associated with each of the HOMCCs occurs is almost identical to the η values of these small basins. In this case, the separation of two monosynaptic basins is not chemically significant, and the two monosynaptic basins can be considered as one disynaptic basin.[17,24,39]

That **THCPC** does not possess pentacoordinate carbons may be due to several factors. The distances between the HOMCCs in all of the species that we investigated consistently range between 1.80 and 1.86 Å, and the three bonds around these carbons nearly lie in the same plane, the sum of the bonds angles ranging between 356° and 360°. It is not unreasonable to expect that the C−X bond lengths play a role in determining deviation from planarity, that is, the deviation angle. When the C−X

TABLE 9: Populations ($\bar{N}$), Basin Variances (σ^2), Relative Fluctuations (λ), Volumes (bohr^3), ELF Values (η) at (3,−3) Critical Points, and Contributions of Other Basins at the Becke3PW91/6-311G(d,p) level for C−X Basins (V(C1,C4), V(C1,P1), V(C1,S1), V(C1,As1), and V(C1,Se1)) of Cations

cation	$\bar{N}$	σ^2	λ	volume	η	contribution analysis (fluctuations) (%)[a]
THCPC	1.93	1.04	0.54	25.25	0.944	15.4 V(H,C1); 14.5 V^1(H,C4); 14.4 V(C2,C4); 14.1V^2(H,C4); 13.5 V(C1,C5); 5.8 C(C1); 4.7 C(C2); 2.4 V(C1)
e-THCPC−PH	1.80	1.03	0.57	27.88	0.927	16.8 V(P1); 15.3 V(H,C1); 14.3 V(C1,P2); 10.5 V(C2,P1); 10.2 V(H,P1); 6.6 C(P1); 6.2 C(C1); 6.0 V(C1,C2); 2.2 V(P2)
a-THCPC−PH	1.85	1.04	0.56	28.61	0.927	16.9 V(P1); 15.8 V(H,C1); 11.1 V(C2,P1); 9.7 V(H,P1); 6.3 C(P1); 5.6 C(C1); 4.1 V(C1);[b] 1.7 V(P2)
THCPC−S	1.63	0.99	0.60	20.06	0.900	18.2 V^1(S1); 17.4 V^2(S1); 13.5 V(H,C1); 11.5 V(C2,S1); 9.4 V(C1,S2); 5.9 C(S1); 5.1 C(C1); 4.8 V(C1), 2.1 V(S2)
e-THCPC−AsH	1.67	1.01	0.61	27.7	0.904	16.9 V(As1); 14.7 V(H,C1); 13.9 V(C1,As2); 12.1 C(As1); 8.8 V(C2,As1); 8.3 V(H,As1); 6.8 V(C1,C3,As2); 5.1 C(C1)
a-THCPC−AsH	1.71	1.03	0.60	28.4	0.907	16.7 V(As1); 15.0 V(H,C1); 14.6 V(C1,As2); 11.9 C(As1); 8.8 V(C2,As1); 8.1 V(H,As1); 6.3 V(C1,C3,As2); 5.2 C(C1)
THCPC−Se	1.57	0.99	0.63	22.0	0.889	16.6 V^1(Se1); 15.3 V^2(Se1); 13.3 V(H,C1); 11.8 V(C1,Se2); 10.6 C(Se1); 4.9 V(C1);[b] 4.8 C(C1); 2.9 V(C3)[b]

[a] The superscripts identify different basins, the C−H basins at C2, C4, and C6 of **THCPC** and the lone pairs of the other cations. [b] Sum of two monosynaptic basins on the same carbon.

distance is close to the distance between the HOMCCs, in the case of cations with X = S, PH, or larger than the HOMCC distance as in the case of the As and Se species, the deviation angles are reduced. This results in an increase in the homoconjugation between carbons. The **THCPC** cation has the shortest C−X bond (1.5 Å) and exhibits the largest devation angle of 25.1° and is far from forming a pentacoordinated species as indicated by the magnitude of the distortion that is required to produce interaction lines (bond paths) between the HOMCCs. To have C−X longer than (or at least close to) the C1−C3, C3−C5, and C1−C5 distances appears to be a requirement for a **THCPC** species to exhibit pentacoordinated carbons. AIM delocalization indices provide additional information. The sum of the DIs of all possible pairs between a carbon atom and other atoms is in the range of 3.90−4.20 with five pairs (two C−C or two C−X pairs and one C−H pair) making the dominant contributions (3.84−4.10). To form additional bond paths to C1, C3, and C5, the DIs of the remaining bonds must decrease to maintain the sum of the DIs at the optimal value because a concomitant increase in the C1−C3, C3−C5, and C1−C5 DIs is necessary. In **THCPC**, the $\delta_{C1,C3(C5)}$ value is only $^1/_2\delta_{C,X}$ or $^1/_2\delta_{C,H}$ When $\delta_{C,X}$ or $\delta_{C,H}$ are reduced as in the case of the substituted **THCPCs**, the DIs between the HOMCCs can increase accordingly with the formation of pentacoordinate carbons. Compared to the HF method, DFT methods appear to reduce charge separation and increase DIs between two atoms with significant charge separations as seen in the comparison of the results obtained at the HF/6-311G(d,p)//Becke3PW91/6-311G(d,p) and Becke3PW91/6-311G(d,p)//Becke3PW91/6-311G(d,p) levels. A similar conclusion can be drawn from an analysis of the ELF basin populations. The populations of the ELF basins around C1, C3, or C5 sum to values from 5.88 to 6.79 electrons (7.02 to 7.40 when the small basins in the C1−C3−C5 plane are taken as a group). These numbers are significantly less than 8. This type of analysis has been used recently to investigate the chemical bonding in so-called hypervalent molecules.[40] Clear differences in the AIM and ELF analyses are seen in the results for **THCPC−S** and **THCPC−Se**. While AIM theory gives the largest DI sums of 4.228 and 4.235 (Table 8) for the HOMCCs of the **THCPC−S** and **THCPC−Se** at Becke3PW91/6-311G(d,p)//Becke3PW91/6-311G(d,p) level, the two species have the smallest ELF basin population sums (5.96 and 5.88) of the series (Table 4). The differences are due to the C−X bonds; while the $\delta_{C,X}$ values (Table 7) are the largest (1.077 and 1.023), the V(C,X) populations (Table 13, Supporting Information) are the smallest (1.63 and 1.57). The lone pair electrons play an important role in these cases. In ELF, lone pairs occupy separated basins, while in AIM theory lone pairs are included in the X atomic basins and thereby contribute to the DIs. Because AIM atoms satisfy the fundamental quantum mechanical relations[10,11] and ELF basins are not proper open systems,[33] AIM theory is the method of choice for investigating delocalization. While discussions on the octet rule are usually based on the dominant pairs around one atom,[41] delocalization can involve any pair of atoms because Fermi correlation is not restricted to the dominant pairs of atoms.[13,14]

The C_{3v} symmetry cations are stabilized by delocalization that mostly involves the electrons in the remote C−C bond of the parent [3.1.0] system. Yet neither AIM nor ELF (the number is about 1−1.5 if the ELF basin populations are summed) analyses find the number of electrons involved to be precisely 2. The AIM DIs show that more than three electrons are delocalized. Delocalization of the two electrons from the remote C−C bond is the driving force for formation of the C_{3v} structure *and this results in the involvement of more bonds/electrons in the delocalization.* This includes the C−X and X−H bonds and the lone pairs on X. These factors have been envoked to explain the existence of two different chair structures for 1-methyl-1-cyclohexyl cation.[42,43] In our systems, the pair of electrons of the remote C−C bond and the equatorial lone pairs of X are keys in determining the structures of the local and global minima on the potential energy surface. The delocalization of two electrons of C−C bond makes the C_{3v} structure the global minimum for the **THCPC** cation. The presence of lone pairs on X makes these C_{3v} structures only local minima for all of the other species.

Isomerization of Cations. Table 10 collects the relative energies for the minima and transition states (TSs), as well as the fold angles. The folding potential energy surfaces for X = CH_2, PH, and S are displayed in Figure 11. They are obtained by full optimization with only the fold angle being fixed. The potentials for X = AsH and Se are very close to those for X = PH and S and are not shown in the figure. When the fold angle of all of the substituted cations is increased, the total energies decrease dramatically after barriers between 3.7 and 24.1 kcal mol^{-1} are overcome. The barriers for **e-THCPC−PH**, **THCPC−S**, **e-THCPC−AsH**, and **THCPC−Se** are low, 3.7, 6.8,

TABLE 10: Relative Energies (kcal mol^{-1}), Fold Angles (deg) and Zero-Point Energies (kcal mol^{-1}) for Minima and Transition States in the Folding Process

	reactant (C_{3v})	TS	product (C_s)
	THCPC		
ΔE	0.0	24.7	14.9
fold angle	87.6	144.0	188.2
ZPE	84.6	82.2	81.5
	e-THCPC−PH		
ΔE	0.0	6.8	−21.4
fold angle	65.9	101.2	154.1
ZPE	48.9	48.4	48.6
	a-THCPC−PH		
ΔE	0.0	24.1	−13.5
fold angle	72.1	141.6	208.5
ZPE	49.7	48.1	49.1
	THCPC−S		
ΔE	0.0	3.7	−57.4
fold angle	69.6	97.3	183.0
ZPE	32.7	32.0	34.0
	e-THCPC−AsH		
ΔE	0.0	7.4	−13.5
fold angle	58.9	102.5	152.2
ZPE	45.4	44.8	45.1
	a-THCPC−AsH		
ΔE	0.0	20.5	−8.1
fold angle	62.8	140.7	209.3
ZPE	45.8	44.7	45.5
	THCPC−Se		
ΔE	0.0	1.5	−59.8
fold angle	62.8	95.0	182.2
ZPE	30.0	29.5	31.7

7.4, and 1.5 kcal mol^{-1}, respectively. On the other hand, **a-THCPC−PH** and **a-THCPC−AsH** have significantly larger barriers of 24.7 and 20.5 kcal mol^{-1}, respectively. Table 11 also includes the net charges of atoms and atom groups for the unfolding process. For each carbocation, the delocalized pair of electrons is localized to form a bicyclo[3.1.0] species; the optimized geometries of **i-THCPC**, **i-e-THCPC−PH**, **i-a-THCPC−PH**, **i-THCPC−S**, **i-e-THCPC−AsH**, **i-a-THCPC−AsH**, and **i-THCPC−Se** are displayed in Figure 2. The e-isomers exhibit two "chair" minima, and the a-isomers exhibit a chair and a "boat" minimum-energy structure. The preference of chair or boat global minima depends on the degree of delocalization of the lone pairs to the cationic center. On the whole, the axial C_{3v} isomers are lower in energy than equatorial species, and axial isomers exhibit higher unfolding barriers as seen in Figure 11.

It is seen that the AIM atomic charges for the reactant and TS are similar, but values for the product cation differ significantly from the reactant and the TS. The changes in populations in the unfolding/isomerization of **THCPC** are small; all of the atoms are nearly neutral. For the substituted species, X2 and X3 lose electrons in going from the reactants through the TSs to the product, while X1 gains electrons. In the products, C3 is the most negatively charged atom, while X2 and X3 are the most positively charged atoms. Table 12 (Supporting Information) gives the delocalization indices, and the ELF basin populations for the unfolding process are collected in Table 13 (Supporting Information). It is obvious that the C1−C2 and C2−C3 interactions become weaker and weaker and the DI decreases from about 0.5 to almost 0 while the DI between C1 and C2 increases to almost 1. Interestingly, the equatorial lone-pair basins on X lose more electrons (Table 13), and as expected, the lone pairs donate more electrons than the V(C−H)s. If equatorial lone pairs are not available, axial lone pairs are effective as well.

An electrostatic/ionic-character effect appears to play a role in stabilizing the isomers and in determining the magnitude of the unfolding/isomerization barriers (Tables 1, 2, 10, and 11). The axial isomers are lower in energy than equatorial isomers by 8.6 and 5.6 kcal/mol for **THCPC−PH** and **THCPC−AsH**, respectively, and exhibit larger charge separations (0.02−0.08 e) and smaller distances between C and X (in the region of 0.02 Å). Inclusion of ZPE corrections did not alter the relative stabilities of the cations. In going from the C_{3v} cations to the transition states, the net charge difference between C3 and X2(X3) decreases from 2.505 to 2.439 for **a-THCPC−PH** and from 1.576 to 1.460 for **a-THCPC−AsH**; on the other hand, the net charge difference between C3 and X2(X3) increases from 2.363 to 2.526 in the case of **e-THCPC−PH** and from 1.507 to 1.535 for **e-THCPC−AsH**. The axial isomers have higher (by 15.3 and 13.1 kcal.mol) unfolding/isomerization barriers. In the case of the substituted species, the bicyclic cations, which are the most stable species, exhibit the largest negative charge at C3 (−0.515 to −1.304 e) and the largest positive charge at X2 and X3 (0.556−1.851 e). **THCPC** does not have significant charge separation (<0.05 e), and it is the only case in which the C_{3v} species is the global minimum.

The ability of $\nabla^2\rho(\mathbf{r})$ and ELF to provide information about the electron pairs has been extensively examined. In general, these two fields are homeomorphic.[44] Comparisons have been made between $\nabla^2\rho(\mathbf{r})$ and one-electron potential (OEP) in terms of their behavior to reproduce atomic shell structures[45,46] and molecular structures.[47] A distinction between OEP and Bohm's quantum potential was also made very recently.[30,48] The absence of atomic valence shells in $\nabla^2\rho$ beyond the third row of the periodic table was shown to manifest itself in the lack of valence shell charge concentrations (VSCCs) in fourth row diatomic molecules.[47] We also find that the VSCCs of the As and Se lone pairs of **e-** and **a-THCPC-AsH** and **THCPC-Se** are absent in $\nabla^2\rho$ plots but are located in the OEP and ELF analyses; it is advantageous to provide OEP and ELF plots for molecules containing elements beyond the third row.

Additional Comments. In the ELF analyses, we find small basins in the HOMCC plane with patterns that are basis-set dependent. Technically, this indicates the localization of electrons, and the assignment of basins based on the gradient of ELF is problematic in the HOMCC. Consequently, it is reasonable to combine all small basins into a single large basin; all of the small basins are shared by three HOMCCs through high delocalization. Similar small basins also exist in the X = O and X = NH cations that we studied, but the results are not included in this paper. Like **THCPC**, the X = O and X = NH cations are not σ,σ-bond homoconjugated species. ELF reproduces the 3c−2e homoconjugation restricted in the HOMCC plane, although the total population of the small basins is less than 2 (1−1.5 e). Needless to say, the 3c−2e homoconjugation proposed here is quite different from the typical 3c−2e bonding found in boron compounds.[49]

Three factors that stabilize the six-membered-ring cations can be identified: (a) hyperconjugation, here we include contributions from adjacent C−X and X−H bonds and lone pairs, (b) 3c−2e homoconjugation, and (c) an electrostatic effect. In **THCPC**, factors a and b are in competition, and the latter provides 14.9 kcal mol^{-1} more stabilization energy. In the substituted cations, the role of lone pairs becomes important. The lone pairs of S and Se are particularly effective in stabilizing the bicyclic cations. In P and As, the lone-pair stabilization

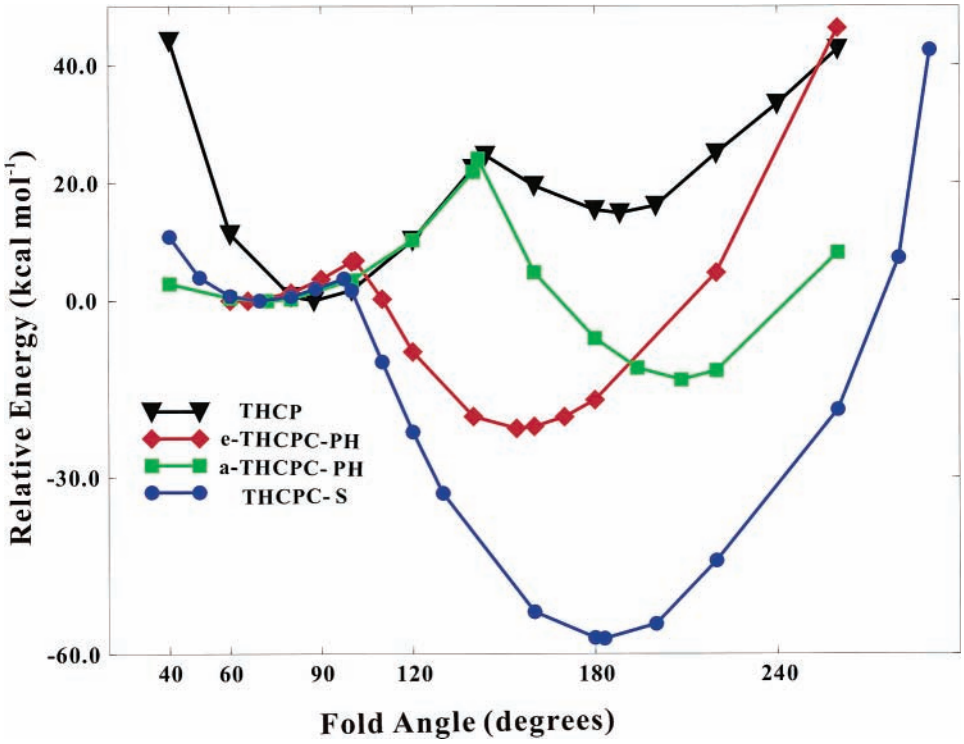

Figure 11. The relationship between the relative energy and the fold angle for **THCPC**, **THCPC−S**, **THCPC−PH**, and **THCPC−S** in the folding process at the Becke3PW91/6-311G(d,p)//Becke3PW91/6-311G(d,p) level.

TABLE 11: Atomic Charges on Atoms in the Folding Process at the Becke3PW91/6-311G(d,p) Level

	reactant	TS	product
	THCPC		
C3	−0.044	0.060	0.093
C1 (or C2)	−0.044	−0.039	−0.026
C5 (or C6)	0.032	0.002	−0.034
C4	0.032	−0.004	−0.019
	e-THCPC−PH		
C3	−0.852	−0.949	−1.290
C1 (or C2)	−0.852	−0.809	−0.915
P2 (or P3)	1.511	1.587	1.822
P1	1.511	1.369	1.330
	a-THCPC−PH		
C3	−0.912	−0.839	−1.304
C1 (or C2)	−0.912	−0.936	−0.919
P2 (or P3)	1.593	1.600	1.851
P1	1.593	1.478	1.326
	THCPC−S		
C3	−0.221	−0.211	−0.515
C1 (or C2)	−0.221	−0.201	−0.170
S2 (or S)	0.376	0.396	0.556
S1	0.376	0.388	0.228
	e-THCPC−AsH		
C3	−0.542	−0.529	−0.677
C1 (or C2)	−0.542	−0.545	−0.564
As2 (or As3)	0.965	1.015	1.055
As1	0.965	0.854	0.816
	a-THCPC−AsH		
C3	−0.564	−0.454	−0.686
C1 (or C2)	−0.564	−0.587	−0.570
As2 (or As3)	1.012	1.006	1.070
As1	1.012	0.916	0.852
	THCPC−Se		
C3	−0.361	−0.344	−0.533
C1 (or C2)	−0.361	−0.388	−0.328
Se2 (or Se3)	0.524	0.484	0.687
Se1	0.524	0.535	0.336

appears to be less effective because the cations remain pyramidal at P and As. Sulfur and selenium substitution leads to a stabilization energy that is 4 times greater than PH and AsH substitution. Nevertheless, stabilization by adjacent lone pairs is always better than 3c−2e homoconjugation; 3c−2e homoconjugation is better than C−X and X−H hyperconjugation. It appears that the orientation of lone pairs is not the key factor determining the relative stabilities of the axial and equatorial isomers and the difference in unfolding/isomerization barriers. It is the stabilization of **a-THCPC−PH** and **a-THCPC−AsH** by the electrostatic effect, the degree of ionic character in the C−X bonds, that makes their experimental observation as σ,σ-bond homoconjugated species a possiblity.

The presence of the relatively long, polarizable C−X bonds increases the "flexibility" of the S-, PH-, S-, AsH-substituted cations. The HOMCCs can approach each other more easily resulting in new bond paths. While the distance between HOMCCs remains almost unchanged (1.832 Å in **THCPC** and 1.778−1.868 Å in substituted cations), the distance between X atoms increases from 2.581 Å in **THCPC** to 3.104−3.560 Å in substituted species. We see that the charge separation between C and X increases in going from **THCPC** (0.076) to the **THCPC−Xs** (0.597−2.363). On the other hand, the V(C,X) basin population decreases in going from **THCPC** (1.93) to the substituted cations (1.57−1.85), and δ(C,X) also decreases from 0.976 in THCPC to 0.781−0.857 in X = PH and AsH species. The slight increase in X = S and Se species comes from the electrons in the lone pairs as pointed out in the preceding text. The ionic character of the C−X bonds is important in the formation of pentacoordinated carbons in the substituted species. To achieve bond paths C1 between C3 and C5, the C1−C3, C3−C5, and C1−C5 DIs must increase. This is only possible if the DIs (covalent character) of the C−X bonds decrease to maintain the sum of the DIs at the HOMCCs at the optimal value as discussed in the section on hypercoordination above.

Conclusions

It is clear that **THCPC** is a σ,σ-no-bond homoconjugated species without pentacoordinated carbons; it is not a hypercarbon

species. In fact, a high-energy distortion is required to convert this species into a "nonclassical" hypercarbon species that exhibits three pentacoordinate carbons. Nevertheless, pentacoordinate species are easily form by replacing the methylenes of **THCPC** by PH, S, AsH, and Se groups. The resulting cations are the first examples of σ,σ-bonded homoconjugated species. Two key requirements must be met: (a) long, polarizable C,X bonds with ionic charatcter are required, and (b) as the DIs between C1−C3, C3−C5, and C1−C5 are increased in the formation of pentacoordinate "cationic" carbons, there must be a concomitant decrease in the DIs to the X atoms to maintain the sum of the DIs at the optimal value.

Acknowledgment. We are indebted to Professor Richard Bader and his research group for helpful discussion. We thank Dr. W. -T. Chan and Professor I. P. Hamilton for providing the code for the OEP that we included in GRIDV2. We gratefully acknowledge grants of CPU time on CRAY T90 at the NIC, Jülich, Germany, and SGI Origin 2000 at Université de Montréal, a center of the Réseau Québécois de Calcul de Haute Performance (RQCHP) computers. We thank the Natural Sciences and Engineering Research Council of Canada for financial support.

Supporting Information Available: Figures 5−7 displaying $\nabla\rho(\mathbf{r})$ in the C1−C2−C3 and C1−X−C2 planes of the compounds and Tables 4−6, 12, and 13 providing the populations, basin variances, relative fluctuations, volumes and ELF values of monosynaptic basins, contributions of other basins, atomic charges, DIs, and basin populations of the compounds. This material is available free of charge via the Internet at http://pubs.acs.org.

References and Notes

(1) Winstein, S. *J. Am. Chem. Soc.* **1959**, *81*, 6524.
(2) Winstein, S.; Sonnenberg, J. *J. Am. Chem. Soc.* **1961**, *83*, 3235, 3244.
(3) Masamune, S.; Sakai, M.; Jones, A. V. K.; Nakashima, T. *Can. J. Chem.* **1974**, *52*, 855.
(4) Olah, G. A.; Prakash, G. K. S.; Rawdah, T. N.; Whittaker, D.; Rees, J. C. *J. Am. Chem. Soc.* **1979**, *101*, 3935.
(5) Haywood-Farmer, J. *Chem. Rev.* **1974**, *74*, 315.
(6) Paquette, L. A. *Angew. Chem., Int. Ed. Engl.* **1978**, *17*, 106.
(7) Childs, R. F. *Acc. Chem. Res.* **1984**, *17*, 347.
(8) Williams, R. V. *Chem. Rev.* **2001**, *101*, 1185.
(9) Olah, G. A.; Prakash, G. K. S.; Williams, R. E.; Field, L. D.; Wade, K. *Hypercarbon Chemistry*; John Wiley & Sons: New York, 1987.
(10) Bader, R. F. W. *Atoms in Molecules-A Quantum Theory*; Oxford University Press: Oxford, U.K., 1990.
(11) Popelier, P. L. A. *Atoms in Molecule. An Introduction*; Pearson Education: Harlow, U.K., 1999.
(12) Becke, A. D.; Edgecombe, K. E. *J. Chem. Phys.* **1990**, *92*, 5397.
(13) Bader, R. F. W.; Stephens, M. E. *J. Am. Chem. Soc.* **1975**, *97*, 7391.
(14) Fradera, X.; Austen, M. A.; Bader, R. F. W. *J. Phys. Chem. A* **1999**, *103*, 304.
(15) Silvi, B.; Savin, A. *Nature* **1994**, *371*, 683.
(16) Noury, S.; Colonna, A.; Savin, A.; Silvi, B. *J. Mol. Struct. (THEOCHEM)* **1998**, *450*, 59.
(17) Savin, A.; Silvi, B.; Colonna, F. *Can. J. Chem.* **1996**, *74*, 1088.
(18) Cremer, D.; Kraka, E.; Slee, T. S.; Bader, R. F. W.; Lau, C. D. H.; Nguyen-Dang, T. T.; MacDougall, P. J. *J. Am. Chem. Soc.* **1983**, *105*, 5069.
(19) Szabo, K. J.; Kraka, E.; Cremer, D. *J. Org. Chem.* **1996**, *61*, 2783.
(20) Cremer, D.; Childs, R. L.; Kraka, E. In *The Chemistry of the cyclopropyl group*; Rappoport, Z., Ed.: John Wiley & Sons Ltd: New York, 1995; Vol. 2, pp 339−410.
(21) Werstiuk, N. H.; Muchall, H. M. *J. Mol. Struct. (THEOCHEM)* **1999**, *463*, 225.
(22) Werstiuk, N. H.; Muchall, H. M. *J. Phys. Chem. A* **2000**, *104*, 2054.
(23) Werstiuk, N. H.; Muchall, H. M.; Noury, S. *J. Phys. Chem. A* **2000**, *104*, 11601.
(24) Werstiuk, N. H.; Wang, Y. G. *J. Phys. Chem. A* **2001**, *105*, 11515.
(25) Frisch, M. J.; Trucks, G. W.; Schlegel, H. B.; Gill, P. M. W.; Johnson, B. G.; Robb, M. A.; Cheeseman, J. R.; Keith, T.; Petersson, G. A.; Montgomery, J. A.; Raghavachari, K.; Al-Laham, M. A.; Zakrzewski, V. G.; Ortiz, J. V.; Foresman, J. B.; Cioslowski, J.; Stefanov, B. B.; Nanayakkara, A.; Challacombe, M.; Peng, C. Y.; Ayala, P. Y.; Chen, W.; Wong, M. W.; Andres, J. L.; Replogle, E. S.; Gomperts, R.; Martin, R. L.; Fox, D. J.; Binkley, J. S.; Defrees, D. J.; Baker, J.; Stewart, J. P.; Head-Gordon, M.; Gonzalez, C.; Pople, J. A. *Gaussian 94*, revision B.3; Gaussian, Inc.: Pittsburgh, PA, 1995.
(26) Frisch, M. J.; Trucks, G. W.; Schlegel, H. B.; Scuseria, G. E.; Robb, M. A.; Cheeseman, J. R.; Zakrzewski, V. G.; Montgomery, J. A., Jr.; Stratmann, R. E.; Burant, J. C.; Dapprich, S.; Millam, J. M.; Daniels, A. D.; Kudin, K. N.; Strain, M. C.; Farkas, O.; Tomasi, J.; Barone, V.; Cossi, M.; Cammi, R.; Mennucci, B.; Pomelli, C.; Adamo, C.; Clifford, S.; Ochterski, J.; Petersson, G. A.; Ayala, P. Y.; Cui, Q.; Morokuma, K.; Malick, D. K.; Rabuck, A. D.; Raghavachari, K.; Foresman, J. B.; Cioslowski, J.; Ortiz, J. V.; Stefanov, B. B.; Liu, G.; Liashenko, A.; Piskorz, P.; Komaromi, I.; Gomperts, R.; Martin, R. L.; Fox, D. J.; Keith, T.; Al-Laham, M. A.; Peng, C. Y.; Nanayakkara, A.; Gonzalez, C.; Challacombe, M.; Gill, P. M. W.; Johnson, B. G.; Chen, W.; Wong, M. W.; Andres, J. L.; Head-Gordon, M.; Replogle, E. S.; Pople, J. A. *Gaussian 98*, revision A.1; Gaussian, Inc.: Pittsburgh, PA, 1998.
(27) Biegler-König, F. W.; Bader, R. F. W.; Tang, T.-H. *J. Comput. Chem.* **1982**, *3*, 317.
(28) Biegler-König, F.; Schönbohm, J. *AIM2000*, version 2.0; Innovation Software: Bielefeld, Germany, 2002.
(29) Cremer, D.; Kraka, E. *Angew. Chem., Int. Ed. Engl.* **1984**, *23* (8), 627.
(30) Chan, W.-T.; Hamilton, I. P. *J. Chem. Phys.* **1998**, *108* (6), 2473.
(31) Matta, C. F. *AIMDELOC*; QCPE0802; Quantum Chemistry Program Exchange, Department of Chemistry, Indiana University: Bloomington, IN.
(32) Noury, S.; Krokidis, X.; Fuster, F.; Silvi, B. *TopMod*; Université Pierre et Marie Curie: Paris, 1997.
(33) Noury, S.; Krokidis, X.; Fuster, F.; Silvi, B. *Comput. Chem.* **1999**, *23*, 597.
(34) Pepke, E.; Murray, J.; Lyons, J.; Hwu, T.-Y. *SciAn*, version 1.21; Alpha: Supercomputer Computations Research Institute: Florida State University, Tallahassee, FL, 1991.
(35) Wang, Y.-G.; Werstiuk, N. H. *J. Comput. Chem.* **2003**, *24* (3), 379.
(36) Sieber, S.; Schleyer, P. V. R.; Otto, A. H.; Gauss, J.; Reichel, F.; Cremer, D. *J. Phys. Org. Chem.* **1993**, *6*, 445.
(37) Honegger, E.; Heilbronner, E.; Schmelzer, A. *Nouv. J. Chim.* **1982**, *6* (11), 519.
(38) Honegger, E.; Heilbronner, E.; Schmelzer, A.; Wang, J.-Q. *Isr. J. Chem.* **1982**, *22* (1), 3.
(39) Calatayud, M.; Andres, J.; Beltran, A.; Silvi, B. *Theor. Chem. Acc.* **2001**, *105* (4−5), 299−308.
(40) Noury, S.; Silvi, B.; Gillespie, R. J. *Inorg. Chem.* **2002**, *41* (8), 2164.
(41) Cioslowski, J.; Mixon, T. *Inorg. Chem.* **1993**, *32*, 3209.
(42) Rauk, A.; Sorensen, T. S.; Maerker, C.; Carneiro, M.; Sieber, S.; Schleyer, P. V. R. *J. Am. Chem. Soc.* **1996**, *118*, 3761.
(43) Rauk, A.; Sorensen, T. S.; Schleyer, P. V. R. *J. Chem. Soc., Perkin Trans. 2* **2001**, 867.
(44) Bader, R. F. W.; Johnson, S.; Tang, T.-H.; Popelier, P. L. A. *J. Phys. Chem.* **1996**, *100*, 15398.
(45) Kohout, M. *Int. J. Quantum Chem.* **2001**, *83*, 324.
(46) Sagar, R. P.; Ku, A. C.; Simith, V. H., Jr. *Can. J. Chem.* **1988**, *66*, 1005.
(47) (a) Levit, C.; Sarfatti, J. *Chem. Phys. Lett.* **1997**, *281*, 157. (b) Hamilton, I. P. *Chem. Phys. Lett.* **1998**, *297*, 261. (c) Levit, C.; Sarfatti, J. *Chem. Phys. Lett.* **1998**, *297*, 263.
(48) Kohout, M. *Int. J. Quantum Chem.* **2002**, *87*, 12.
(49) Burckhardt, A.; Wedig, U.; von Schnering, H. G.; Savin, A. *Z. Anorg. Allg. Chem.* **1993**, *619*, 437.